

Raman spectral study of silicon nanowires: High-order scattering and phonon confinement effects

Rong-ping Wang

*Laboratory of Optical Physics, Institute of Physics & Center for Condensed Matter Physics,
Chinese Academy of Sciences, Beijing 100080, China*

Guang-wen Zhou

*Beijing Laboratory of Electron Microscopy, Center for Condensed Matter Physics, Chinese Academy of Sciences,
P.O. Box 2724, Beijing 100080, China*

Yu-long Liu and Shao-hua Pan

*Laboratory of Optical Physics, Institute of Physics & Center for Condensed Matter Physics,
Chinese Academy of Sciences, Beijing 100080, China*

Hong-zhou Zhang and Da-peng Yu

Department of Physics, National Key Laboratory of Mesoscopic Physics, Peking University, Beijing 100864, China

Ze Zhang

*Beijing Laboratory of Electron Microscopy, Center for Condensed Matter Physics, Chinese Academy of Sciences,
P.O. Box 2724, Beijing 100080, China*

(Received 23 December 1998; revised manuscript received 21 December 1999)

Raman-scattering spectra of silicon nanowires (SiNW's) with different diameters were obtained at room temperature. The Raman peaks of SiNW's were found to shift and to broaden with decreasing diameter of the SiNW's. In addition to the fundamental phonon modes, overtone and combination modes were also observed and identified according to the selection rules of overtone and combination bands. A phonon confinement model was used to explain the experimental results of observed phonon modes. The results show that the confinement effect becomes more obvious when the SiNW diameter is less than 22 nm. The present results should be of benefit to the applications of SiNW's.

I. INTRODUCTION

Material science has witnessed substantial progress in the synthesis, characterization, and understanding of materials of mesoscopic scale in recent years. Using a variety of techniques, it is possible to synthesize materials with dimensions ranging from a few angstroms to several nanometers. The electronic, magnetic, optical, and chemical properties of these materials have been found to be very different from those of the bulk form and to depend sensitively on size, shape, and composition. In silicon science and technology, the desire for the integration of optoelectronics devices with silicon microelectronics has led to the search for Si-based materials and structures that emit light with high quantum efficiency. Crystalline silicon (*c*-Si) does not show efficient light emission at room temperature, because of its band structure with an indirect band gap of ~ 1.1 eV and a small exciton binding energy (~ 15 meV). One promising approach to overcoming the indirect nature of optical transition in silicon is the relaxation of the *k* selection rule due to the spatial confinement in low-dimensional Si nanostructures. As a consequence, increasing interest in the low-dimensional structures with possible applications in optoelectronics has given rise to several attempts to synthesize of quasi-one-dimensional crystalline nanowires with the sp^3 -bonded structure. Recently, the successful synthesis of Si nanowires

(SiNW's) by laser ablation has stimulated intensive interest in this one-dimensional nanostructured material.^{1,2} Due to its low dimension and high surface-to-volume ratio, SiNW's are expected to exhibit unusual confinement effects on electrical and optical properties. Preliminary investigations revealed that the physical properties of SiNW's are different from those of Si (Refs. 3 and 4), Ge (Refs. 5 and 6), and GaAs (Refs. 7 and 8) whiskers with diameters ranging from micrometers to millimeters. The size-confinement effect has a strong influence on the band structure of SiNW's. The electronic and optical properties of the SiNW's are modified through size confinement and spatial correlation effects. In addition to the electronic properties of the nanowires, increasing interest has also been given to studies of the lattice-dynamical properties, including a substantial amount of Raman and infrared spectroscopy work. These spectroscopic investigations should, in principle, lead to further understanding of these nanostructures.⁹⁻¹¹ Raman scattering is very sensitive to the lattice microstructure. Phonon frequencies and scattering intensities determined by Raman spectroscopy can lead to conclusions concerning microscopic parameters such as bonding and structure as well as deviations from the ideal crystalline counterpart. In this paper, we report Raman-scattering spectroscopic studies on the lattice properties of SiNW's. Raman spectra of SiNW's with different diameters were measured at room temperature. In addition to the fundamental modes, some other bands have also been observed in SiNW's, most of which can be explained

by overtone and combination modes of SiNW's on the basis of the factor-group analysis. A phonon confinement model is employed to explain the Raman shift of phonon modes of SiNW's. We use the term *phonon confinement* to describe the size confinement effect on lattice vibration (phonon) wave functions. Moreover, the term *confinement* refers to phonon confinement in the rest of the paper, except when a specific statement is given. It was found that, when the diameter of SiNW's decreases to 22 nm, the confinement effect begins to play an important role in determining the Raman shift. It can be expected that the present results should be of benefit to potential applications of SiNW's.

II. EXPERIMENTS

The SiNW's were synthesized by the same oven-laser ablation method used for BN nanotubes¹² as described in the experimental details of the synthesis in our previous work.¹³ Conventional transmission electron microscope (TEM) analysis of SiNW's was performed using a Philips-CM12 electron microscope. High-resolution electron microscopy (HREM) was conducted by using a JEM-2010 high-resolution electron microscope operating at 200 kV with a point-to-point resolution of 0.194 nm. The micro-Raman backscattered spectra were recorded by using a Renishaw 2000 spectrometer with a 514.5-nm wavelength Ar-ion laser. The spectral resolution was 1 cm^{-1} . The spot size of the focused incident light was approximately 1 mm^2 on the sample. In order to clarify the effect caused by sample heating, the Raman spectra of the SiNW's illuminated by different laser powers from 0.5 to 5 mW (corresponding to laser power densities from 0.05 to 0.5 J/cm^2) on the sample were recorded.

III. RESULTS AND DISCUSSION

The SiNW's samples with different diameters used for the Raman-scattering study were synthesized under various ambient pressures.¹⁴ The size distribution and mean diameter of each sample were calculated from TEM images by measuring hundreds of diameters of SiNW's in many TEM images taken from different typical parts of the sample. Figure 1(a) is a typical TEM image showing the morphology of the SiNW's with uniform distribution of diameters. The average diameter of the SiNW's is about 15 nm and the length ranges from a few micrometers to millimeters. The selected-area electron diffraction pattern taken from the SiNW's is shown in the inset on the upper left of the micrograph. Figure 1(b) is the HREM image of a single SiNW along the [110] axis, the two-dimensional lattice image revealing the single-crystalline structure, which shows the representative structural features of SiNW's. Many structural defects such as {111} twin and stacking faults are observable from the HREM image. Analysis of HREM images obtained from many SiNW samples shows that the Si(111) planes are parallel to or have little orientation deviation ($<5^\circ$) from the axis of the nanowires. The SiNW surfaces are coated by thin amorphous silicon oxide layers about 3 nm in thickness owing to surface oxidation. The amorphous silicon oxide skins may be important for SiNW's because it not only makes the dangling bonds saturated and the surface passivated but can

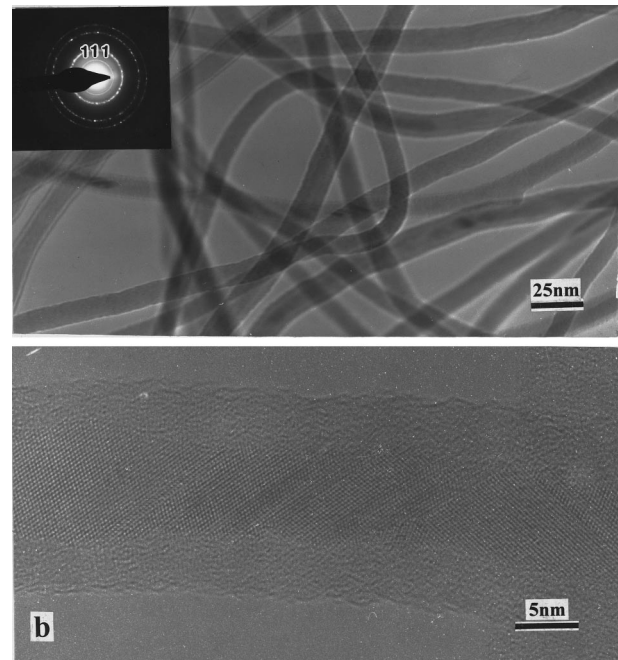


FIG. 1. (a) Typical TEM micrograph showing a general view of the morphology of the SiNW's. (b) HREM image of a single SiNW along the [110] axis.

also help keep the carriers confined in the SiNW's.

The Raman spectra for SiNW's with diameters of 10, 15, and 21 nm and for bulk *c*-Si were recorded. The results are shown in Fig. 2(a). From the figure we can see that the Ra-

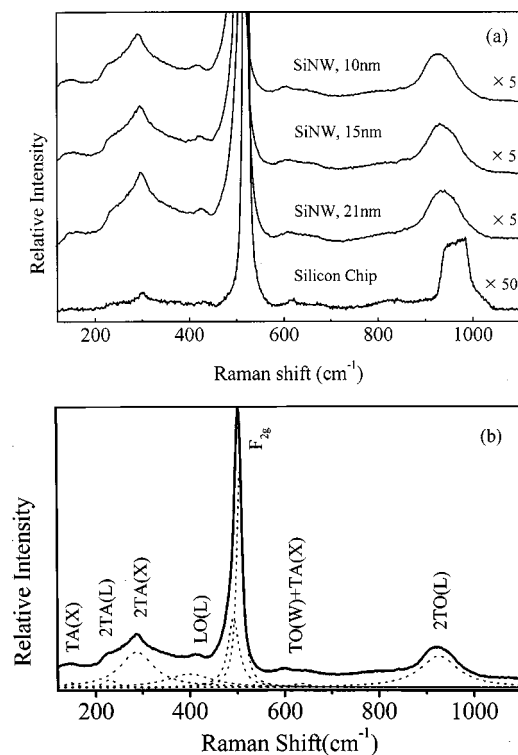


FIG. 2. (a) Raman spectra for SiNW's with diameter of 10, 15, and 21 nm and for bulk *c*-Si. (b) Full profile of a Raman spectrum of the SiNW's with a diameter of 10 nm and its decomposition. The solid line represents the recorded Raman spectrum, and the dashed lines are its decomposition.

man peaks around 150, 300, 520, and 930 cm^{-1} shift towards lower frequencies and their linewidths become larger with decreasing SiNW diameter. Furthermore, more phonons appear in the Raman spectra of SiNW's compared with those of *c*-Si, and the intensities of these phonons increase with decreasing SiNW diameter. Their origin will be discussed in a later part of this paper.

From Fig. 2 we can also see that the overall spectra of SiNW's with different diameters are quite similar except for the magnitudes of the Raman intensity, shift, and broadening. Thus, in order to be more specific in the following detailed analysis for the Raman spectra, we choose the spectrum of SiNW's with a diameter of 10 nm as an example and compare it with that of bulk *c*-Si. Figure 2(b) shows the full profile of such a Raman spectrum and its decomposition. From Fig. 2(a) we can see that a Raman peak at 519 cm^{-1} with a full width at half maximum (FWHM) of 4 cm^{-1} can be found in the Raman spectrum of *c*-Si. This is ascribed to the scattering of the first-order optical phonon of *c*-Si. In addition, two broad peaks at 302 and 964 cm^{-1} are also observed. Those are assigned to the overtones of TA(*X*) and TO(*L*), respectively. In the Raman spectrum of the SiNW's of diameter 10 nm, it can be seen that the first-order optical phonon is shifted to 505 cm^{-1} from 519 cm^{-1} and the FWHM of this phonon mode is broadened to 13 cm^{-1} from 3.5 cm^{-1} as compared with *c*-Si. In addition to the Raman scattering of the first-order optical phonon, some other Raman-scattering peaks are also observed in the SiNW's.

It is well known that effects of sample heating caused by laser radiation and compressive stress give rise to a frequency shift of the Raman peaks. Similarly, the confinement effect also results in a frequency shift of the Raman peaks of SiNW's. Therefore, it is necessary to analyze the relative contributions of different mechanisms to the Raman shift.

First, the effect of sample heating due to laser irradiation was considered. We recorded the Raman spectra of SiNW's (of diameter 10 nm) excited by laser powers of 5, 2.5, and 0.5 mW. The Raman peak for the first-order optical mode is located at 505.8 cm^{-1} (505.1 cm^{-1}) when the sample is illuminated by a laser power of 0.5 mW (2.5 mW), and the peak shifts to 493 cm^{-1} when the laser power increases to 5 mW. Thus the effect of increasing laser power within 2.5 mW (corresponding to a laser power density of 0.25 J/cm^2) of the Raman peak can be neglected. Moreover, from the peak positions and cross sections of the Stokes (ω_S) and anti-Stokes (ω_{AS}) components, the temperature of the sample heated by laser radiation can be estimated by the following equation:¹⁵

$$n(\omega_S)I_S = \{n(\omega_{AS}) + 1\}I_{AS}, \quad (1)$$

where I_S and I_{AS} are, respectively, the cross sections of the Stokes and anti-Stokes components, $n(\omega) = 1/[\exp(\hbar\omega/k_B T) - 1]$ is the Bose-Einstein thermal factor, T is the sample temperature, and k_B is Boltzmann's constant. The calculated values of the sample temperature are 35.9, 46.7, and 89.2 $^\circ\text{C}$ for the samples heated by the laser radiation with a power of 0.5, 2.5, and 5 mW, respectively. Thus the effect of increasing laser power within 2.5 mW on the temperature is small. The above analysis indicates that the laser radiation only causes a small temperature increase and has very little influence on the Raman shift of the SiNW's when the incident laser

power is less than 2.5 mW. The recorded Raman spectra analyzed in this paper was excited by a laser power of less than 2.5 mW (0.25 J/cm^2). Therefore, the effect of sample heating on the Raman shift will not be considered in the following discussion.

The samples of SiNW's are powderlike deposits in which nanowires are only weakly bound and in loose contact with each other. Therefore, it is likely that a free-boundary condition for SiNW's is realized. On the other hand, according to the HREM image, there is a thin layer of amorphous SiO_x on the surface of the SiNW's, which may cause stress in the nanowires. According to the data of x-ray diffraction of SiNW's, the lattice parameter of the SiNW's is equal to $a_{\text{SiNW's}} = 0.5435$ nm, which is 0.4% larger than its bulk counterpart of $a_{\text{Si}} = 0.541$ nm. This indicates a slight lattice expansion of the SiNW structure compared with that of bulk *c*-Si. This slight lattice distortion leads to a minute stress, which results in a small Raman shift determined by the following equation:¹⁶

$$\Delta\omega = -n\nu\omega_0 \frac{a - a_0}{a_0}, \quad (2)$$

where n is the dimensionality of the materials, ν is the Gruneisen constant, and ω_0 is the Raman peak position of the corresponding bulk material. Based on Eq. (2), the Raman shift caused by the stress is about 2 cm^{-1} . Taking into consideration the experimental error, we think the effect of compressive stress on the Raman spectra of SiNW's is negligible.

The above discussions indicate that the Raman shift mainly comes from other mechanisms, among which we think the most important one is the confinement effect in SiNW's. It is well known that the Raman spectrum of a crystal may contain numerous combination and overtone bands because of the anharmonicity effect. In an ideal crystal, the correlation length is infinite, and hence the phonon eigenstates are plane waves. Therefore, the usual $k=0$ momentum selection rule of the first-order Raman spectrum can be satisfied. As the crystallite is reduced to nano scale, the most important effect on the Raman spectra is that the crystal momentum conservation rules will be relaxed. This allows phonons with wave vector $|k| = |k'| \pm 2\pi/L$ to participate in the first-order Raman scattering. Here k' is the wave vector of the incident light and L is the size of the crystal. The phonon scattering will not be limited to the center of the Brillouin zone, and phonon dispersion near the zone center must also be considered. As a result, the symmetry-forbidden modes will be observed, in addition to the shift, broadening, and asymmetry of the first-order optical phonon. This can explain why more phonons appear in the Raman spectrum of SiNW's. The related assignment of the peaks in the Raman spectra of the SiNW's is shown in Fig. 2(b). The assignment is based on the analysis of the irreducible representations of the $k=0$ vibrational modes. In the case of combination of modes, the characters of the vibration representations are given by^{16,17}

$$\frac{1}{g(q)} \sum_R \chi^{(\nu)}(R^{-1}) \chi_q^{(m)}(R) \chi_{-q}^{(n)}(R) = n, \quad (3)$$

TABLE I. The observed and theoretical peak positions, FWHM, and assignments for *c*-Si, and SiNWs with diameters of 21, 15, and 10 nm, respectively.

Sample	Observed peaks (cm ⁻¹)		Theoretical peaks (cm ⁻¹)		Assignments
	Position	FWHM	Position	FWHM	
<i>c</i> -Si	301.8±4	15±1.1	301.2	118	2TA(<i>X</i>)
	519.4±0.9	4±0.5	519.4	4.5	<i>F</i> _{2<i>g</i>}
	964±2.1	62.5±1.4	966.1	59.9	2TO(<i>L</i>)
21-nm SiNW	298±2.5	66.2±0.6	300.6	159.6	2TA(<i>X</i>)
	514.9±0.8	6.8±2.3	517.7	4.7	<i>F</i> _{2<i>g</i>}
15-nm SiNW	935±2.7	80.6±2.8	969.1	62.0	2TO(<i>L</i>)
	295±1.6	68.1±1.4	298.9	165.6	2TA(<i>X</i>)
10-nm SiNW	511.2±0.4	10.3±2	514.3	7.5	<i>F</i> _{2<i>g</i>}
	932±1.1	87.5±1.4	971.4	82.4	2TO(<i>L</i>)
10-nm SiNW	291±1.3	68.9±2.2	294.4	168.6	2TA(<i>X</i>)
	505.1±0.6	17±1.7	509.8	13.1	<i>F</i> _{2<i>g</i>}
	926±1.1	88.6±0.3	973.1	82.6	2TO(<i>L</i>)

In the case of overtone bands, the characters of vibration representations are given by¹⁷

$$\frac{1}{2g(q)} \sum_R \{ \chi^\nu(R^{-1}) \chi_q^{(m)}(R) \chi_q^{(m)}(Z^{-1}RZ) + \chi^\nu[(RZ)^{-1}] \chi_q^{(m)}[(RZ)^2] \} = n, \quad (4)$$

where n is an integer and the quantity $\chi^\nu(R)$ denotes the characters of irreducible representation for the symmetry operation R of the point group. According to the above selection rule, the assignment of the Raman peaks of SiNW's is shown in Fig. 2(b). It is well known that the second-order Raman spectrum is due to the inelastic scattering of a photon by two phonons. Since their fundamental phonon modes are shifted and their FWHM's are broadened, the high-order modes of SiNW's are also shifted and broadened. According to the experimental results, the phonon modes of TA(*X*), 2TA(*L*), 2TA(*X*), LO(*L*), and TO(*W*) + TA(*X*) are shifted to the lower frequencies. This is consistent with the analysis of breakdown of the $k=0$ selection rule, i.e., along the same dispersion curve as the fundamental modes. However, the frequency of 2TO(*L*) is also redshifted in this experiment. This is not consistent with the theoretical analysis based on the breakdown of the $k=0$ selection rule. There may be some other mechanism to cause the redshift for this mode.

In the following section, we make some simple calculations, based on the confinement model, for the Raman shift and broadening of SiNW's. As pointed out above, the phonon wave function is partially confined to the volume of the crystallite. The first-order Raman spectrum $I(\omega)$ can be described by the following equation:^{18,19}

$$I(\omega) = \int \frac{d^3q |C(0, \mathbf{q})|^2}{[\omega - \omega(\mathbf{q})]^2 + (\Gamma/2)^2}, \quad (5)$$

where $\omega(k)$ represents the phonon dispersion, Γ is the natural linewidth, and $C(0, \mathbf{k})$ is the Fourier coefficient that de-

scribes the phonon confinement. Because the SiNW's are column-shaped crystals, the Fourier coefficients can be written as follows:^{18,19}

$$|C(0, \mathbf{k}_1, \mathbf{k}_2)|^2 \cong e^{-k_1^2 L_1^2 / 16\pi^2} e^{-k_2^2 L_2^2 / 16\pi^2} \left| 1 - \operatorname{erf} \left(\frac{ik_2 L_2}{\sqrt{32\pi}} \right) \right|^2, \quad (6)$$

where L_1 and L_2 are, respectively, the diameter and length of the SiNW's. The length of the nanowires is much larger than the diameter, which means that the confinement effect mainly occurs along the diameter direction of the nanowires. We therefore let the integration for L_2 range from zero to infinity. The HREM investigation indicates that (111) planes are parallel to the axis of the nanowires or have little orientation deviation from the axis of the nanowires. Accordingly, three obvious Raman modes for 2TA(*X*), *F*_{2*g*}, and 2TO(*L*) are calculated using the different dispersion curves. The results of the peak position and FWHM obtained by this model are listed in Table I. It is found that the redshift of phonon frequency and broadening of the FWHM of the Raman peaks are more obvious with the decrease of the diameter of the nanowires. As a comparison, the measured peak position and FWHM's for these three Raman modes are also listed in Table I, from which it is evident that a general agreement between the experimental and calculated Raman shift and FWHM for 2TA(*X*) and *F*_{2*g*} but not 2TO(*L*) modes [see the discussions below Eq. (4)]. However, some discrepancies are also found in Table I. First, the experimental peak positions deviate slightly from the theoretical prediction. According to the experimental results, the Raman peak positions of the first-order optical phonon are 505, 511, and 515 cm⁻¹ for SiNW's with diameters of 10, 15, and 21 nm. However, the calculated peak positions are 509.8, 514.3, and 517.7 cm⁻¹, respectively. Obviously, the discrepancy between the calculated and experimental peak positions becomes larger with decreasing diameter of SiNW's. According to the high-resolution TEM observations, it is found that there is a thin amorphous silicon oxide layer on the surface of the SiNW's, which has a broad Raman peak at 480 cm⁻¹. This peak has

significant effects on the F_{2g} peak of SiNW's. [the decomposed Raman peak in Fig. 2(b) at 480 cm^{-1} is due to the same reason.] Also, there is a contribution from the phonon density of state to the Raman spectrum, resulting in the stronger baseline and broader Raman peak. This kind of contribution becomes more important when the amorphous layer becomes thicker. Moreover, the fraction of surface to volume increases with decreasing diameter of SiNW's. This translates into a stronger effect of the amorphous layers in the Raman spectrum, resulting in increased Raman-scattering intensity and shift with decreasing SiNW diameter. On the other hand, the crystalline core is smaller than that of the TEM morphology observation, and this gives rise to a larger experimental Raman shift than the calculated value based on TEM data. Other effects such as deviation from the diamond structure and carrier-induced strain effect may also lead to a Raman shift, which contributes to this discrepancy. Moreover, the fact that the F_{2g} phonon shows a larger asymmetrical shape when the diameter of SiNW's is less than 20 nm indicates that a surface phonon with frequency slightly lower than that of the F_{2g} optical phonon may exist to the left side of the F_{2g} Raman peak.^{20,21} However, our present work gives no direct proof that we have observed the surface phonon. A detailed discussion on the surface phonon is beyond the present study. Second, it is obvious that the calculated FWHM of the Raman peak is much smaller than that of the measured values, as seen from Table I. The reason for this is that there are more physical mechanisms that cause peak broadening. In the SiNW samples, there are many structure defects such as stacking defaults, twins, and high-order twin boundaries, according to our high-resolution TEM observations.²² These structural defects are important because they are not only closely related to the growth process, but also deeply influence the physical properties of the SiNW's. The effect of lattice distortion and the phonon strain field around the core of the defects will become increasingly important when the size of the materials is reduced to nanoscale. The existence of these defects in the SiNW's has profound influence on the Raman spectra and can give rise to the peak broadening of the Raman spectra.

In order to show more clearly the above-mentioned confinement effects on the Raman shift and broadening, a graphic representation of the observed and calculated results for the F_{2g} phonon mode is presented in Fig. 3. We can clearly see the trend that the Raman peaks have a large red-

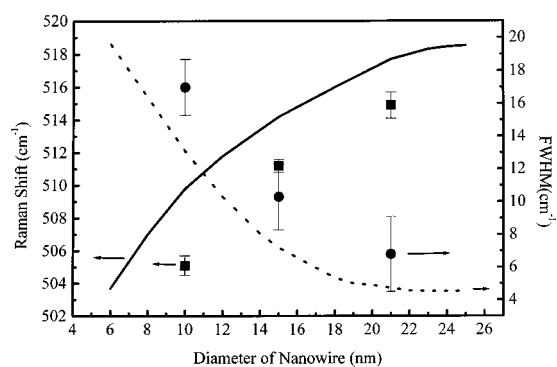


FIG. 3. Comparison between the measured and calculated Raman shift and FWHM of the first-order optical phonon mode for SiNW's with different diameters.

shift and broadening as the SiNW diameter becomes smaller. Furthermore, we can see from Fig. 3 that the confinement effect is obvious when the diameter of SiNW's is less than 18 nm. However, when the diameter is larger than 22 nm, the position and FWHM of the F_{2g} Raman peaks are almost the same as those for *c*-Si. This suggests that 22 nm can be considered as a phonon confinement length, compared with the electronic (excitonic) confinement length of about 5 nm as shown in Fig. 1 of Ref. 23.

IV. CONCLUSIONS

The Raman spectra of SiNW's with different diameters have been recorded and analyzed. All the Raman peaks have a redshift and the Raman peaks are broadened compared with bulk *c*-Si. In addition to the fundamental phonon modes, overtone and combination modes were also observed and assigned based on the selection rules. The shift and broadening of three obvious Raman peaks have been calculated on the basis of the confinement model. The results are in agreement with the experimental data for 2TA(X) and F_{2g} modes, indicating that the relaxation of the wave-vector selection rule plays an important role in SiNW's. Some possible origins accounting for the discrepancy between the calculated and experimental data are discussed. The present study on phonon confinement effects should be useful to further investigations of physical properties (e.g., electron-phonon interaction and scattering) of SiNW's and be of benefit to their applications.

¹D. P. Yu *et al.*, Solid State Commun. **105**, 403 (1998).

²Alfredo M. Morales and Charles M. Lieber, Science **279**, 208 (1998).

³R. S. Wagner and W. C. Ellis, Appl. Phys. Lett. **4**, 89 (1964).

⁴E. I. Givargizov, J. Cryst. Growth **32**, 20 (1975).

⁵E. I. Givargizov, J. Cryst. Growth **20**, 217 (1973).

⁶G. A. Boostma and H. J. Gassen, J. Cryst. Growth **10**, 223 (1971).

⁷K. Hiruma *et al.*, Appl. Phys. Lett. **59**, 431 (1991).

⁸K. Hiruma *et al.*, J. Appl. Phys. **77**, 447 (1995).

⁹A. Ingale and K. C. Rustagi, Phys. Rev. B **58**, 7197 (1998).

¹⁰J. Zi, K. M. Zhang, and X. D. Xie, Phys. Rev. B **58**, 6712 (1998).

¹¹A. M. Rao *et al.*, Science **275**, 187 (1997).

¹²D. P. Yu *et al.*, Appl. Phys. Lett. **72**, 1966 (1998).

¹³D. P. Yu *et al.*, Appl. Phys. Lett. **72**, 3458 (1998).

¹⁴H. Z. Zhang *et al.*, Appl. Phys. Lett. **73**, 4088 (1998).

¹⁵W. Hayes and R. London, *Scattering of Light by Crystals* (Wiley, New York, 1978).

¹⁶P. Bruesch, *Phonons: Theory and Experiments I—Lattice Dynamics and Models of Interatomic Forces* (Springer, Berlin, 1982).

¹⁷E. B. Wilson, J. C. Decius, and I. C. Cross, *Molecular Vibrations—The Theory of Infrared and Raman Vibrational Spectra* (Dover, New York, 1980).

¹⁸H. Richter, Z. P. Wang, and L. Ley, Solid State Commun. **39**, 625 (1981).

- ¹⁹I. H. Campbell and P. M. Fauchet, *Solid State Commun.* **58**, 739 (1986).
- ²⁰S. Hayashi and H. Kanamori, *Phys. Rev. B* **26**, 7079 (1982).
- ²¹S. Hayashi S and K. Yamamoto, *Superlattices Microstruct.* **2**, 581 (1986).
- ²²G. W. Zhou, Z. Zhang, Z. G. Bai, S. Q. Feng, and D. P. Yu, *Appl. Phys. Lett.* **73**, 677 (1998).
- ²³T. Takagahara and K. Takeda, *Phys. Rev. B* **46**, 15 578 (1992).